Surface Chemistry

Deutsche Ausgabe: DOI: 10.1002/ange.201509021
Internationale Ausgabe: DOI: 10.1002/anie.201509021

Methanol Conversion into Dimethyl Ether on the Anatase TiO_2(001) Surface

Feng Xiong[+], Yan-Yan Yu[+], Zongfang Wu, Guanghui Sun, Liangbing Ding, Yuekang Jin, Xue-Qing Gong, and Weixin Huang**

Abstract: *Exploring reactions of methanol on TiO_2 surfaces is of great importance in both C1 chemistry and photocatalysis. Reported herein is a combined experimental and theoretical calculation study of methanol adsorption and reaction on a mineral anatase TiO_2(001)-(1 × 4) surface. The methanol-to-dimethyl ether (DME) reaction was unambiguously identified to occur by the dehydration coupling of methoxy species at the fourfold-coordinated Ti^{4+} sites (Ti_{4c}), and for the first time confirms the predicted higher reactivity of this facet compared to other reported TiO_2 facets. Surface chemistry of methanol on the anatase TiO_2(001)-(1 × 4) surface is seldom affected by co-chemisorbed water. These results not only greatly deepen the fundamental understanding of elementary surface reactions of methanol on TiO_2 surfaces but also show that TiO_2 with a high density of Ti_{4c} sites is a potentially active and selective catalyst for the important methanol-to-DME reaction.*

The conversion reactions of methanol are among the most important reactions in C1 chemistry, wherein the dehydration of methanol into dimethyl ether (DME) catalyzed by solid acids, including γ-Al_2O_3, zeolite, hetero-polyacid, and composite oxides, receives increasing interest because DME has emerged as a star molecule in energy and environmental chemistry, and plays an alternative role to methanol.[1–4] As a representative and versatile oxide catalyst, TiO_2 has been explored as catalysts for methanol conversion.[5,6] The photocatalytic conversion of methanol over TiO_2 has been a hot topic in photocatalysis.[7] These reports have motivated fundamental studies of methanol adsorption and reaction on TiO_2 surfaces that mostly employed TiO_2 single crystals as a model surfaces.[8–18]

Among various types of TiO_2 facets anatase TiO_2(001) is of particular interest. Several theoretical calculations suggested the anatase TiO_2(001) surface to be very reactive,[19–23] however, this reactivity has not been experimentally proved. Meanwhile, experimental studies of its surface structure and reactivity are very limited, with most reports on anatase TiO_2(001) thin films[24–27] and a few on mineral anatase TiO_2(001) surfaces.[25,28] Herein we report a combinational thermal desorption spectra (TDS), X-ray photoelectron spectroscopy (XPS), and density-function theory (DFT) calculation study of methanol adsorption and reaction on a mineral anatase TiO_2(001) surface. The methanol-to-DME reaction was unambiguously identified to occur by the dehydration coupling of a methoxy species (CH_3O) at the fourfold-coordinated Ti^{4+} sites (Ti_{4c}) of the anatase TiO_2-(001)-(1 × 4) surface, and thus, for the first time confirmed the predicted higher reactivity of this facet than other reported TiO_2 facets.

Experiments were performed in a Leybold stainless-steel ultrahigh vacuum (UHV) chamber with a base pressure of 1.2×10^{-10} mbar.[16] Prior to experiments, an anatase TiO_2-(001) single crystal (5 × 5 × 0.5 mm^3), purchased from MaTeck, was cleaned by repeated cycles of Ar ion sputtering, oxidation at 800 K, and annealing at 900 K. Figure 1 A shows the Ti 2p and O 1s XPS spectra of a clean anatase TiO_2(001) surface, giving the Ti $2p_{3/2}$ and O 1s binding energies respectively at 462.3 and 533.6 eV, which are both 2.8 eV higher than the corresponding Ti $2p_{3/2}$ and O 1s binding energies of a clean rutile TiO_2(110) surface. This difference could be attributed to

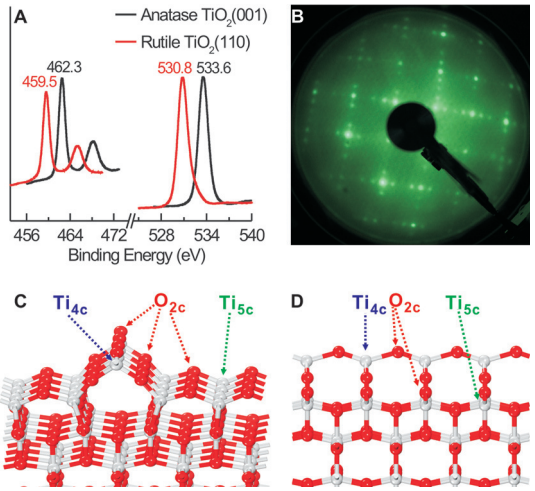

Figure 1. A) Ti 2p and O 1s XPS spectra of clean anatase TiO_2(001) and rutile TiO_2(110) surfaces. B) LEED pattern of a clean anatase TiO_2(001) surface (E_p = 170 eV). C,D) Front view and side view of the proposed model of the anatase TiO_2(001)-(1 × 4) surface.

[*] F. Xiong,[+] Z. Wu, G. Sun, L. Ding, Y. Jin, Prof. Dr. W. Huang
Hefei National Laboratory for Physical Sciences at the Microscale, CAS Key Laboratory of Materials for Energy Conversion, and Department of Chemical Physics
University of Science and Technology of China
Jinzhai Road 96, Hefei 230026 (P. R. China)
E-mail: huangwx@ustc.edu.cn
Y.-Y. Yu,[+] Prof. Dr. X.-Q. Gong
Key Laboratory for Advanced Materials, Centre for Computational Chemistry and Research Institute of Industrial Catalysis
East China University of Science and Technology
Meilong Road 130, Shanghai 200237 (P. R. China)
E-mail: xgong@ecust.edu.cn
[+] These authors contributed equally to this work.
Supporting information for this article is available on the WWW under http://dx.doi.org/10.1002/anie.201509021.

the fact that the rutile TiO_2(110) surface is more easily reduced than the anatase TiO_2(001) surface and thus exhibits a better conductivity.[25] However, the XPS spectra of the clean anatase TiO_2(001) surface remained unchanged upon X-ray irradiation during XPS measurements (see Figure S1 in the Supporting Information), suggesting the absence of a differential charge effect and a continuous charge accumulation. We thus calibrated the binding energies of measured XPS spectra by setting the Ti $2p_{3/2}$ binding energy to 459.5 eV to facilitate their assignments. The low-energy electron diffraction (LEED) pattern of a clean anatase TiO_2(001) surface (Figure 1B) shows a sharp (1×4) reconstructed pattern. This pattern demonstrates the formation of a reconstructed anatase TiO_2(001)-(1×4) surface upon treatment, and the proposed structure is schematically illustrated in Figures 1C and D.[24,25] The Ti^{4+} cations on the ridge and terrace of the anatase TiO_2(001)-(1×4) surface are respectively Ti_{4c} and fivefold-coordinated Ti^{4+} (Ti_{5c}), whereas the surface O anions are all twofold-coordinated (O_{2c}).

Figure 2 shows TDS spectra of 0.5 L CH_3OH exposed at 115 K and 10 L CH_3OH exposed at 320 K on the anatase TiO_2(001)-(1×4) surface. Corresponding TDS spectra of various CH_3OH exposures are shown in Figures S2 and S3.

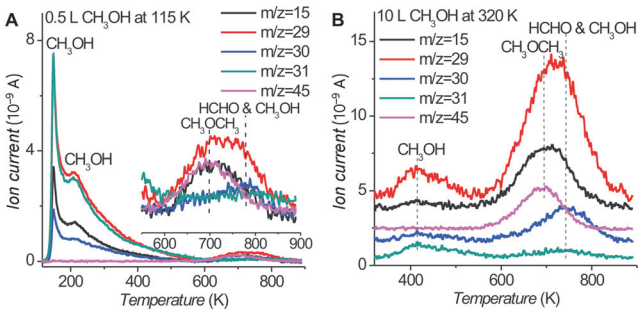

Figure 2. TDS spectra of 0.5 L CH_3OH exposed at 115 K (A) and 10 L CH_3OH exposed at 320 K (B) on the clean anatase TiO_2(001)-(1×4) surface. The inset in Figure 2A shows the zoom-in TDS spectra between 550 and 900 K.

the anatase TiO_2(001)-(1×4) surface and its formation is enhanced at elevated temperatures. Of particular interest is the observation of obvious and simultaneous desorption peaks of the $m/z = 45$, 15, and 29 signals at 700 K. After careful examination of all likely products (see Figure S4), the desorption peaks of these signals at 700 K were identified to arise from the desorption of DME. The amount of desorbed DME is larger after 10 L CH_3OH exposure, at 320 K, than after 0.5 L CH_3OH exposure at 115 K. The production of DME from methanol adsorption has not been observed on other reported TiO_2 single-crystal surfaces,[12–18] except on a seriously restructured rutile TiO_2(001)-{114} facetted surface.[11] It is noteworthy that the observed products from CH_3OH adsorption and reaction on our anatase TiO_2(001)-(1×4) surface are quite similar to those on anatase TiO_2 powders,[29,30] suggesting that the surface sites having similar structures to those on anatase TiO_2(001)-(1×4) surface should dominate the surface chemistry of methanol on anatase TiO_2 powders.

The surface species formed upon CH_3OH adsorption and reaction on the anatase TiO_2(001)-(1×4) surface were examined with XPS. Figure 3 shows C 1s XPS spectra of

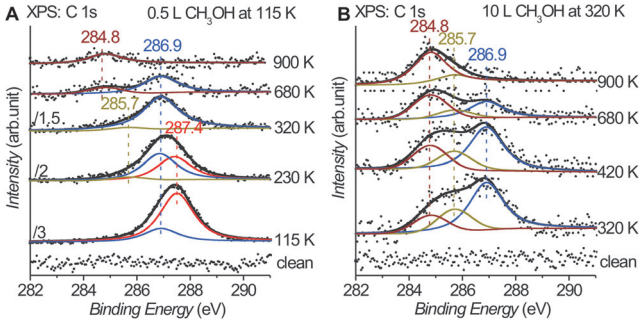

Figure 3. C 1s XPS spectra of 0.5 L CH_3OH exposed at 115 K (A) and 10 L CH_3OH exposed at 320 K (B) on the clean anatase TiO_2(001)-(1×4) surface followed by annealing at the indicated temperatures. The scatter data and solid lines represent original data and fitted results, respectively.

CH_3OH desorption peaks at 150, 210, and 415 K can be respectively assigned to the desorption of CH_3OH(a) multilayer, the desorption of CH_3OH(a) monolayer, and the recombinative desorption of adsorbed methoxy species [CH_3O(a)]. Similar results were previously reported for CH_3OH adsorption on other TiO_2 single-crystal surfaces.[11–18] Simultaneously desorption peaks of HCHO, inferred by the higher intensity of the $m/z = 30$ signal relative to the $m/z = 31$ signal, and CH_3OH were also observed at 780 K after 0.5 L CH_3OH exposure at 115 K, and both features grow and shift to 750 K after 10 L CH_3OH exposure at 320 K. Such features were not observed for CH_3OH adsorption on vacuum-annealed rutile TiO_2(110),[12–16] TiO_2(001),[11] or TiO_2(011)-(2×1) surfaces,[18] but were observed on anatase TiO_2(101),[17] facetted rutile TiO_2(001)-{011},[11] and oxidized rutile TiO_2-(110) surfaces,[12,15] and attributed to the disproportionation reaction between two CH_3O(a) species. Thus CH_3O(a), with a high thermal stability, forms upon CH_3OH adsorption on 0.5 L CH_3OH exposed at 115 K and 10 L CH_3OH exposed at 320 K on the anatase TiO_2(001)-(1×4) surface followed by annealing at indicated temperatures. As shown in Figure 3A, 0.5 L of CH_3OH exposed at 115 K gives a C 1s spectrum with a dominant component at 287.4 eV and a shoulder at 286.9 eV, which can be assigned to adsorbed CH_3OH(a) and CH_3O(a), respectively.[16] Upon annealing, the CH_3OH(a) component reduces at 230 K and disappears at 320 K. The CH_3O(a) component keeps increasing until 320 K and then reduces at 680 K and disappears at 900 K. A weak component at 285.7 eV, assigned to a CH_x species[31] (see Figure S5), emerges at 320 K and slightly grows at 680 K and disappears at 900 K. And a carbon component at 284.8 eV appears at 680 K and grows at 900 K. As shown in Figure 3B, 10 L CH_3OH exposed at 320 K gives a C 1s spectrum consisting of CH_3O(a), CH_x, and carbon components. Upon annealing, the CH_3O(a) component keeps decreasing and disappears at 900 K, as does the CH_x component. However, the carbon

component keeps growing. The tiny CH_x component observed at 900 K should arise from the decomposition of CH_3OH in the residual gases of our UHV chamber because of the relatively large CH_3OH exposure during the XPS measurements. It is noteworthy that X-ray radiation during the XPS measurements does not affect the surface reactions of CH_3O(a) (see Figure S6). C 1s XPS spectra of various CH_3OH exposures at 115 K (see Figure S7) and 320 K (see Figure S8) demonstrate that the decomposition of CH_3OH into CH_3O(a) and carbon is preferred at very low coverages at 115 K, and the molecular adsorption gradually dominates with the coverage increasing while CH_3OH always decomposes into CH_3O(a), CH_x, and carbon at 320 K.

The above XPS and TDS results of CH_3OH adsorption and reaction on the anatase TiO_2(001)-(1×4) surface demonstrate the unprecedented complex surface reactions of CH_3OH on TiO_2 single-crystal surfaces. CH_3OH can decompose into CH_3O(a), adsorbed CH_x species, and carbon at temperatures as low as 115 K. Upon heating, CH_3O(a) can undergo the recombination reaction to produce CH_3OH at 415 K, the dehydration coupling reaction to produce important CH_3OCH_3 at 700 K, the disproportionation reaction to produce CH_3OH and HCHO at 750–780 K, and decomposition into carbon. These results unambiguously prove the higher catalytic activity of the anatase TiO_2(001)-(1×4) surface relative to other reported TiO_2 single crystal surfaces, as predicted by previous theoretical calculations.[19–23]

The dominant surface reaction between 420 and 680 K after CH_3OH exposure at 320 K is the dehydration coupling reaction of CH_3O(a) to produce DME (Figure 2B). Estimated from the peak intensity decrease between the corresponding C 1s XPS spectra of the surfaces annealed at 420 and 680 K (Figure 3B), about 55% of CH_3O(a) on the surface underwent the dehydration coupling reaction. The production of DME and CH_3OH/HCHO are clearly controlled by the bimolecular surface reactions of CH_3O(a). Therefore, by leading-edge analysis of second-order desorption spectra employing the fragments at $m/z = 45$ (exclusively arising from DME) and $m/z = 30$ (exclusively arising from CH_3OH and HCHO), shown in Figure 2A, the surface reactions barriers of the dehydration coupling reaction of CH_3O(a) to produce CH_3OCH_3 and the disproportionation reaction of CH_3O(a) to produce CH_3OH and HCHO on the anatase TiO_2(001)-(1×4) surface were estimated to be about 99 kJ mol^{-1} (1.03 eV) and 142 kJ mol^{-1} (1.43 eV), respectively.

DFT calculations were performed to understand the adsorption and surface reactions of CH_3OH on the anatase TiO_2(001)-(1×4) surface. Figure 4 shows the most stable calculated adsorption configurations of CH_3OH at the Ti_{4c} and Ti_{5c} sites with different coverage with respect to the total number of surface Ti sites. At the Ti_{4c} sites, CH_3OH dissociates with the most stable configuration, thus giving an adsorption energy as large as −3.14 eV at a 0.05 ML coverage, and no stable configuration of molecularly adsorbed CH_3OH(a) could be identified. Three configurations of dissociative adsorption are similarly stable at a 0.1 ML coverage, and configurations of dissociative adsorption and mixed dissociative and molecular adsorption become similarly stable at higher coverages. The dissociation of CH_3OH at

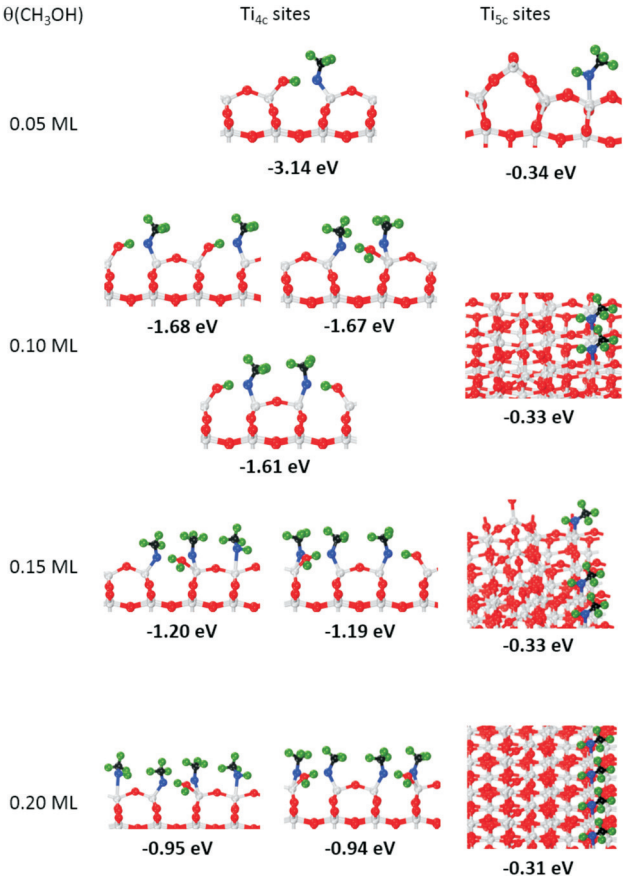

Figure 4. The most stable, calculated adsorption configurations with average adsorption energies for CH_3OH at the Ti_{4c} and Ti_{5c} sites of the anatase TiO_2(001)-(1×4) surface. The grey, red, blue, black, and green spheres represent Ti, O of TiO_2, O of CH_3OH, C, and H atoms, respectively.

the Ti_{4c} sites was found to result in the breaking of Ti_{4c}–O bonds. The average adsorption energy of CH_3OH at the Ti_{4c} sites decreases with the CH_3OH coverage. At the Ti_{5c} sites, the molecular adsorption of CH_3OH is always more stable and the average adsorption energy does not vary much with the coverage. Stable configurations of dissociative adsorption of CH_3OH at the Ti_{5c} sites could be identified (see Figure S9) but the average adsorption energy is much lower than that of molecular adsorption. It is noteworthy that in our structural model the CH_3OH coverages calculated with respect to the individual Ti_{4c} and Ti_{5c} sites are as 5 and 1.25 times that calculated with respect to the total number of the Ti_{4c} and Ti_{5c} sites, respectively. On the basis of these calculation results, Ti_{4c} on the ridge is much more reactive than Ti_{5c} on the terrace, and CH_3OH preferentially dissociates at the Ti_{4c} sites, but molecularly adsorbs at the Ti_{5c} sites. Thus CH_3O(a) experimentally observed in our XPS results are located at the Ti_{4c} sites.

The reaction pathways and energy profiles of the observed bimolecular dehydration coupling reaction and disproportionation reaction of CH_3O(a) were explored by DFT calculations at a 0.1 ML CH_3OH coverage. Two separate CH_3O(a) species, in the configuration with an average adsorption

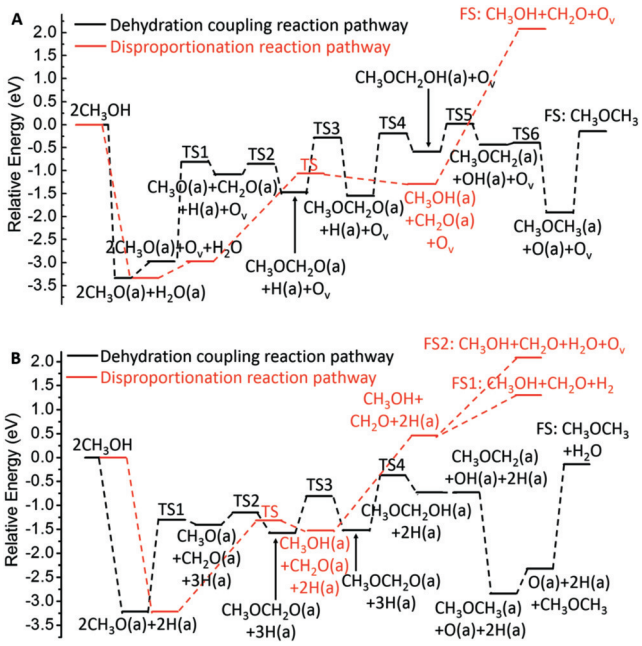

Figure 5. Calculated energy profiles of the bimolecular dehydration coupling reaction and disproportionation reaction of $CH_3O(a)$ at the Ti_{4c} sites of the anatase $TiO_2(001)$-(1×4) surface (0.1 ML CH_3OH coverage): A) the configuration with an average adsorption energy of −1.67 eV and B) the configuration with an average adsorption energy of −1.61 eV.

energy of −1.68 eV, were found not to undergo the bimolecular surface reaction. With the configuration consisting of an average CH_3OH adsorption energy of −1.67 eV (see Figure 5 A and Figure S10), surface reactions are initiated by the desorption of $H_2O(a)$ formed by dissociative CH_3OH adsorption, and simultaneously a surface oxygen vacancy is created. The desorption of molecularly chemisorbed $H_2O(a)$ from the surface was experimentally observed in the water TDS spectra following CH_3OH exposures at 115 K (see Figure S2). During the dehydration coupling reaction to produce DME, one $CH_3O(a)$ firstly dehydrogenates to produce $CH_2O(a)$ with a barrier of 2.16 eV, and then $CH_2O(a)$ facilely couples with the other $CH_3O(a)$ to form $CH_3OCH_2O(a)$ which subsequently undergoes a series of low-barrier surface reactions to form $CH_3OCH_3(a)$. $CH_3OCH_3(a)$ desorbs from the surface with a barrier of 1.77 eV, thus producing gaseous DME and recovering the original surface. During the disproportionation reaction, two $CH_3O(a)$ species undergo a H-transfer reaction to form $CH_3OH(a)$ and $CH_2O(a)$ with a barrier of 1.91 eV, and their desorption to produce the final products needs to overcome a large barrier of 3.37 eV because of the creation of an oxygen vacancy.

During the dehydration coupling reaction to produce DME from the configuration with an average CH_3OH adsorption energy of −1.61 eV (see Figure 5 B and Figure S11), one $CH_3O(a)$ firstly dehydrogenates to produce $CH_2O(a)$ with a barrier of 1.95 eV, and then $CH_2O(a)$ facilely couples with the other $CH_3O(a)$ to form $CH_3OCH_2O(a)$, which subsequently undergoes a series of low-barrier surface reactions to form $CH_3OCH_3(a)$. And $CH_3OCH_3(a)$ facilely desorbs from the surface to produce gaseous DME, and the remaining two H(a), in the form of a hydroxy group, and an O atom react to produce gaseous H_2O with a barrier of 2.18 eV, thus recovering the original surface. For the disproportionation reaction, two $CH_3O(a)$ species undergo a H-transfer reaction to form $CH_3OH(a)$ and $CH_2O(a)$ with a barrier of 1.9 eV, and they desorb to produce the CH_3OH and CH_2O with a barrier of 1.99 eV, and the remaining two H(a) atoms, in the form of hydroxy groups, preferentially recombine to produce gaseous H_2, thus recovering the original surface.

The above DFT calculation results demonstrate that the bimolecular dehydration coupling reaction and disproportionation reaction of $CH_3O(a)$ at the Ti_{4c} sites both involve elementary surface reactions with activation energies of about 2 eV, but their very high thermal stability allow the occurrence of both reactions, as experimentally observed. The dehydration coupling reaction of methanol to DME is slightly exothermic while the disproportionation reaction to formaldehyde is more endothermic. Meanwhile, the disproportionation reaction pathways involve a step with a barrier of 3.37 eV. These DFT calculation results qualitatively agree with our experimental observations that DME, the product of the dehydration coupling reaction with an activation energy of 1.03 eV, is produced at lower temperatures than CH_3OH and CH_2O, which are the products of the disproportionation reaction having an activation energy of 1.43 eV. Therefore, TiO_2 which exposes a high density of Ti_{4c} sites can be expected to be an active and selective catalyst for the important methanol-to-DME reaction.

Water adsorption has been demonstrated to affect the adsorption and surface reaction of methanol on TiO_2 single-crystal surfaces.[8,9] In the TDS spectra of water adsorption on a clean anatase $TiO_2(001)$-(1×4) surface at 115 K (see Figure S12), four water desorption features evolve with the increasing water exposure: hydroxy group recombination peak at about 400 K, desorption peak of $H_2O(a)$ chemisorbed at Ti sites at 270 K, desorption peak of $H_2O(a)$ chemisorbed at O sites at 195 K, and multilayer water desorption peak at 170 K. Similar water TDS results were observed for water adsorption on the rutile $TiO_2(110)$ surface with surface bridging bonded oxygen vacancies where water dissociation occurred.[32] For water adsorption on stoichiometric rutile $TiO_2(110)$ and anatase $TiO_2(101)$ surfaces,[32,33] only desorption peaks of $H_2O(a)$ on Ti sites, $H_2O(a)$ on O sites, and multilayer water were observed. Thus the TDS results demonstrate the water dissociation on the anatase TiO_2-(001)-(1×4) surface at 115 K, thus agreeing with previous synchrotron radiation-excited core-level photoelectron spectroscopy results.[34] DFT calculations were performed for water adsorption on a clean anatase $TiO_2(001)$-(1×4) surface with different water coverages (see Figures S13 and S14). At the Ti_{4c} sites, H_2O preferentially dissociates at low coverage and both dissociatively and molecularly adsorb at large coverage. At the Ti_{5c} sites, the molecular adsorption of H_2O is always preferred. The calculated adsorption energies of H_2O on the clean anatase $TiO_2(001)$-(1×4) surface are also similar to those of methanol. Similar DFT calculation results were previously reported for water and methanol adsorption on an anatase $TiO_2(001)$-(1×1) surface.[21]

Figure 6 shows TDS spectra of the adsorption of 0.02 L CH_3OH on anatase $TiO_2(001)$-(1×4) surfaces pre-exposed to 0.01 L and 0.1 L H_2O at 115 K. The anatase $TiO_2(001)$-(1×4) surface preadsorbed with 0.01 L H_2O at 115 K has hydroxy groups at the Ti_{4c} sites and H_2O(a) chemisorbed at the Ti_{5c} sites, whereas that preadsorbed with 0.1 L H_2O at 115 K has hydroxy groups at the Ti_{4c} sites, H_2O(a) chemisorbed at the Ti_{5c} sites, and H_2O(a) chemisorbed at the O sites. The desorption traces of CH_3OH, CH_3OCH_3, and HCHO are identical to those following the corresponding individual methanol adsorption on the clean surface. The desorption peaks of molecularly adsorbed water appear at slightly lower temperatures and are slightly stronger than those following corresponding individual water adsorption on clean surface. Meanwhile, the TDS spectra of CH_3OH, CH_3OCH_3, HCHO, and H_2O, after 0.02 L methanol adsorption on a 0.1 L water-precovered surface, are identical to those after 0.1 L water adsorption on 0.02 L methanol-precovered surface (see Figure S15). Therefore, co-chemisorbed water has little influence on the surface chemistry adsorption and surface reactions of methanol on the anatase $TiO_2(001)$-(1×4) surface, while co-adsorbed methanol exerts repulsive interactions on molecularly adsorbed water. The enhanced desorption peaks of molecularly adsorbed water for coadsorption of methanol and water over individual water adsorption suggest the transformation of some hydroxy groups, formed by water dissociation at the Ti_{4c} sites, into molecularly adsorbed water. Similar results were also observed for coadsorption of methanol and water on the rutile $TiO_2(110)$ surface and CH_3OH adsorption on hydroxylated rutile and anatase TiO_2 powders.[12,30,35–38]

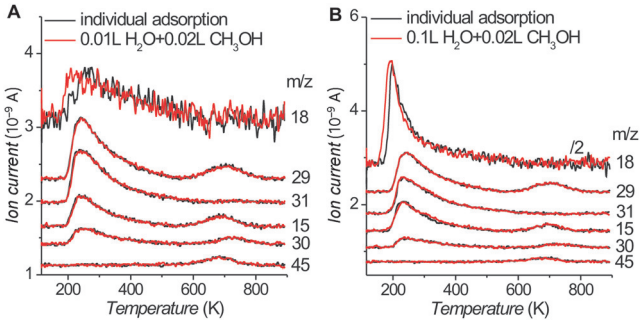

Figure 6. TDS spectra of 0.02 L CH_3OH exposed on anatase TiO_2-(001)-(1×4) surfaces precovered by 0.01 L (A) and 0.1 L (B) H_2O at 115 K. Corresponding TDS spectra of individual H_2O and CH_3OH exposures are also included.

In summary, our results of combined experimental and theoretical calculation studies unambiguously demonstrate that methanol facilely dissociates at the Ti_{4c} sites of the anatase $TiO_2(001)$-(1×4) surface to form strongly adsorbed methoxy groups. These methoxy groups undergo the dehydration coupling reaction to produce DME. The chemisorption and surface reactions of methanol on the anatase $TiO_2(001)$-(1×4) surface is not affected by co-chemisorbed water. These results not only greatly deepen the fundamental understanding of methanol chemistry and TiO_2 catalysis but also predict TiO_2 exposing a high density of Ti_{4c} sites as potentially active and selective catalysts for the important methanol-to-DME reaction.

Acknowledgments

This work was financially supported by National Basic Research Program of China (2013CB933104), National Natural Science Foundation of China (21525313, 21173204, U1332113, 21322307), Chinese Academy of Sciences (KJZD-EW-M03), MOE Fundamental Research Funds for the Central Universities (WK2060030017, WD1313009), and Collaborative Innovation Center of Suzhou Nano Science and Technology.

Keywords: density functional calculations · ethers · heterogeneous catalysis · surface chemistry · titanium

How to cite: *Angew. Chem. Int. Ed.* **2016**, *55*, 623–628
Angew. Chem. **2016**, *128*, 633–638

[1] J. Sun, G. Yang, Y. Yoneyama, N. Tsubaki, *ACS Catal.* **2014**, *4*, 3346–3356.
[2] G. A. Olah, A. Goeppert, G. K. S. Prakash, *J. Org. Chem.* **2008**, *73*, 487–498.
[3] W. Song, D. M. Marcus, H. Fu, J. O. Ehresmann, J. F. Haw, *J. Am. Chem. Soc.* **2002**, *124*, 3844–3845.
[4] P. Tian, Y. Wei, M. Ye, Z. Liu, *ACS Catal.* **2015**, *5*, 1922–1938.
[5] M. Xu, J. H. Lunsford, D. W. Goodman, A. Bhattacharyya, *Appl. Catal. A* **1997**, *149*, 289–301.
[6] R. M. Ladera, J. L. G. Fierro, M. Ojeda, S. Rojas, *J. Catal.* **2014**, *312*, 195–203.
[7] M. A. Henderson, I. Lyubinetsky, *Chem. Rev.* **2013**, *113*, 4428–4455.
[8] U. Diebold, *Surf. Sci. Rep.* **2003**, *48*, 53–226.
[9] M. A. Henderson, *Surf. Sci. Rep.* **2011**, *66*, 185–297.
[10] C. L. Pang, R. Lindsay, G. Thornton, *Chem. Rev.* **2013**, *113*, 3887–3948.
[11] K. S. Kim, M. A. Barteau, *Surf. Sci.* **1989**, *223*, 13–32.
[12] M. A. Henderson, S. Otero-Tapia, M. E. Castro, *Faraday Discuss.* **1999**, *114*, 313–329.
[13] B. Li, J. Zhao, K. Onda, K. D. Jordan, J. Yang, H. Petek, *Science* **2006**, *311*, 1436.
[14] Q. Guo, C. Xu, Z. Ren, W. Yang, Z. Ma, D. Dai, H. Fan, T. K. Minton, X. Yang, *J. Am. Chem. Soc.* **2012**, *134*, 13366.
[15] K. R. Phillips, S. C. Jensen, M. Baron, S. C. Li, C. M. Friend, *J. Am. Chem. Soc.* **2013**, *135*, 574–577.
[16] Q. Yuan, Z. Wu, Y. Jin, L. Xu, F. Xiong, Y. Ma, W. Huang, *J. Am. Chem. Soc.* **2013**, *135*, 5215–5219.
[17] C. Xu, W. Yang, Q. Guo, D. Dai, M. Chen, X. Yang, *J. Am. Chem. Soc.* **2014**, *136*, 602–605.
[18] X. Mao, Z. Wang, X. Lang, Q. Hao, B. Wen, D. Dai, C. Zhou, L. M. Liu, X. Yang, *J. Phys. Chem. C* **2015**, *119*, 6121–6127.
[19] M. Lazzeri, A. Vittadini, A. Selloni, *Phys. Rev. B* **2001**, *63*, 155409.
[20] M. Lazzeri, A. Selloni, *Phys. Rev. Lett.* **2001**, *87*, 266105.
[21] X. Q. Gong, A. Selloni, *J. Phys. Chem. B* **2005**, *109*, 19560–19562.
[22] X. Q. Gong, A. Selloni, A. Vittadini, *J. Phys. Chem. B* **2006**, *110*, 2804–2811.
[23] A. Vittadini, M. Casarin, A. Selloni, *Theor. Chem. Acc.* **2007**, *117*, 663–671.

[24] G. S. Herman, M. R. Sievers, Y. Gao, *Phys. Rev. Lett.* **2000**, *84*, 3354 – 3357.
[25] Y. Liang, S. Gan, S. Chambers, E. Altman, *Phys. Rev. B* **2001**, *63*, 235402.
[26] T. Ohsawa, I. V. Lyubinetsky, M. A. Henderson, S. A. Chambers, *J. Phys. Chem. C* **2008**, *112*, 20050 – 20056.
[27] Y. Wang, H. Sun, S. Tan, H. Feng, Z. Cheng, J. Zhao, A. Zhao, B. Wang, Y. Luo, J. Yang, J. G. Hou, *Nat. Commun.* **2013**, *4*, 2214.
[28] G. Durinck, H. Poelman, P. Clauws, L. Fiermans, J. Vennik, G. Dalmai, *Solid State Commun.* **1991**, *80*, 579.
[29] K. S. Kim, M. A. Barteau, W. E. Farneth, *Langmuir* **1988**, *4*, 533 – 543.
[30] E. A. Taylor, G. L. Griffin, *J. Phys. Chem.* **1988**, *92*, 477 – 481.
[31] J. M. Vohs, M. A. Barteau, *Surf. Sci.* **1989**, *221*, 590 – 608.
[32] M. B. Hugenschmidt, L. Gamble, C. T. Campbell, *Surf. Sci.* **1994**, *302*, 329 – 340.
[33] G. S. Herman, Z. Dohnalek, N. Ruzycki, U. Diebold, *J. Phys. Chem. B* **2003**, *107*, 2788 – 2795.
[34] J. Blomquist, L. E. Walle, P. Uvdal, A. Borg, A. Sandell, *J. Phys. Chem. C* **2008**, *112*, 16616 – 16621.
[35] I. Carrizosa, G. Munuera, S. Castanar, *J. Catal.* **1977**, *49*, 265 – 277.
[36] Y. Suda, T. Morimoto, M. Nagao, *Langmuir* **1987**, *3*, 99 – 104.
[37] G. A. M. Hussein, N. Sheppard, M. I. Zaki, R. B. Fahim, *J. Chem. Soc. Faraday Trans. 1* **1991**, *87*, 2655 – 2659.
[38] C.-y. Wang, H. Groenzin, M. J. Shultz, *J. Am. Chem. Soc.* **2004**, *126*, 8094 – 8095.

Received: September 25, 2015
Published online: November 23, 2015

